EFFECTS OF CONSOLIDATION ON THE UNDRAINED COMBINED *VHM* CAPACITY OF SPUDCANS

R. Ragni*, B. Bienen and M.J. Cassidy
Centre for Offshore Foundation Systems and ARC CoE for Geotechnical Science and Engineering
UNIVERSITY OF WESTERN AUSTRALIA

D. Mašín
Institute of Hydrogeology, Engineering Geology and Applied Geophysics
CHARLES UNIVERSITY OF PRAGUE

D. Wang
Shandong Provincial Key Laboratory of Marine Environment and Geological Engineering
OCEAN UNIVERSITY OF CHINA

* *Corresponding author:* raffaele.ragni@uwa.edu.au

ABSTRACT
The installation of jack-up platforms involves a first stage where the spudcan foundations are penetrated into the seabed for several diameters in depth. When installed in fine-grained soils, this usually results in the accumulation of excess pore pressures. Once the installation is completed, the undrained spudcan capacity under combined vertical, horizontal and moment (*VHM*) loading is evaluated as a function of the maximum vertical load achieved during the undrained installation process. However, this procedure neglects the potential gain in combined *VHM* capacity resulting from a period of load-hold, which typically takes place prior to operations.
The paper quantifies the enhancement of the undrained combined capacity due to consolidation during such load-hold periods, through a combination of numerical and centrifuge experimental tools. Kaolin clay was used in this study as it offers consolidation characteristics that allow a wide range of behaviour to be investigated, with more silty natural soils featuring similar characteristics in the field. The increase in *VHM* capacity is evaluated and described as non-uniform among the loading directions.

KEY WORDS: Jack-up; Spudcan; Consolidation; Combined capacity; Hypoplasticity; Numerical modelling; Centrifuge.

INTRODUCTION

Throughout their lifetime, jack-up platforms undergo different loading scenarios. During the installation stage the circular footings located at the end of each leg, known as spudcans, are subjected to a prevalent vertical loading *V*. However, once installed and in operational conditions, horizontal and moment loading *HM* arising from the metocean actions of winds, waves and currents must be also taken into account.

When installing such platforms in soils characterised by low values of coefficient of consolidation, it is important to keep in mind the role played by the soil drainage properties. As the spudcan is initially penetrated into the soil, some degree of excess pore pressure will be generated, due to the undrained nature of the process. However, either expected or unexpected pauses of the pre-loading operations may lead to partial dissipation of such excess pore pressures and a consequent consolidation of the soil around the spudcan, which may be significant in silty soils in the field. Clearly, the phenomenon of dissipation is not confined to the installation stage, but will continue to take place even upon complete installation of the jack-up; although the pre-load is removed, the self-weight of the structure will continue to foster consolidation. In these circumstances, a reduction in the void ratio can be thus expected, with consequent generalised strengthening and stiffening of the soil.

ISO (2015)[1] provides guidelines for the estimation of the undrained combined *VHM* capacity of spudcans. Briefly, this can be estimated as a function of the vertical preload V_0 achieved during installation and the depth of spudcan installation *w*. A resulting so-called yield surface in the three-dimensional *VHM* loading space can be determined, which envelopes all the admissible loading states (Figure 1).

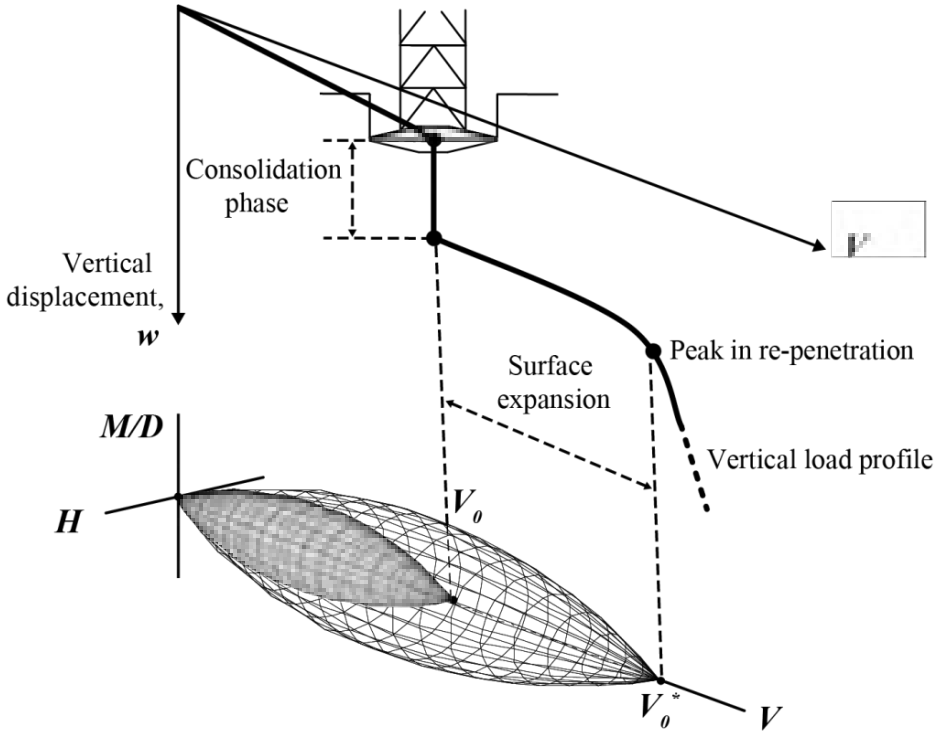

Figure 1: Three-dimensional *VHM* yield surface and its expansion due to consolidation.

Butterfield & Ticof (1979)[2], Schotman (1989) [3] and Nova & Montrasio (1991)[4], among the others, introduced the idea of macro-element to evaluate settlements and rotations of shallow and deep foundations. A yield surface was involved in the formulation of full macro-element models to describe the combined bearing capacity of the footing in the *VHM* loading space. Dean et al. (1997)[5], Cassidy & Houlsby (1999)[6], Bienen et al. (2006)[7] and Salciarini & Tamagnini (2009)[8] proposed *VHM* force-resultant models for spudcans and shallow circular foundations in sand, where fully drained behaviour can be assumed. Martin & Houlsby (2000[9], 2001[10]) and Zhang et al. (2011[11], 2013[12]) focused instead on the response in clay, where undrained soil behaviour is observed.

No technical instructions are provided in the ISO (2015)[1] guidelines regarding the possible influence of consolidation on the spudcan bearing capacity, and in particular how it may affect both size and shape of the yield surface. However, previous studies from Ragni et al. (2015)[13] on spudcan installation in fine grained material highlighted a clear connection between period of load-hold and hence consolidation and the resulting increased spudcan vertical bearing capacity to V_0^*. By extension, the *VHM* yield surface is expected to be enlarged also (Figure 1).

The main purpose of this study is to evaluate the increase in spudcan combined *VHM* capacity, using kaolin clay as a well-researched material that features consolidation characteristics allowing a range of behaviour to be investigated in the centrifuge, and establish whether the same or different improvement is to be expected in different loading directions. The combined capacity will be tested in undrained conditions to simulate a storm

event, since this is the expected foundation response when considering the rate at which such metocean actions are applied.

A combination of numerical and experimental techniques was implemented to study the problem. First, large deformation and small strain numerical analyses on the finite element code Abaqus/Standard allowed the problem to be investigated in a timely and economic fashion, with centrifuge experimental results validating the numerical findings.

NUMERICAL MODEL

LDFE ANALYSES FOR SPUDCAN PENETRATION

An appropriate description of the problem as illustrated in Figure 1 requires the modelling of spudcan penetration to a certain depth, followed by the consolidation stage. This involves large vertical penetration and results in a high degree of shearing and remoulding in the soil. Therefore, an excessive mesh distortion can be expected when simulating the problem numerically, if a Large Deformation Finite Element (LDFE) approach is not employed. In this case, a Remeshing and Interpolation Technique with Small Strain (RITSS, Hu & Randolph 1998[14], Wang et al. 2015[15]) strategy was adopted: consecutive small strain analyses, associated with a periodic mapping of the field variables and soil domain remeshing, successfully simulated the entire penetration and following consolidation. Once the target depth w was reached, the consolidation stage was performed by holding the load for a given time. Simulation of coupled effective stress-pore fluid analyses was necessary to track the generation of excess pore pressures during penetration and following dissipation during consolidation.

HYPOPLASTIC CONSTITUTIVE MODEL

The hypoplastic constitutive model for structured clays (Mašín 2007[16], 2014[17]) was identified as suitable for the full simulation of the installation, consolidation and the following undrained *VHM* loading, given its ability to simulate (i) coupled stress-pore fluid analyses, and (ii) the soil remoulding experienced in the large-amplitude penetration.

Hypoplasticity is an approach to the non-linear constitutive modelling of geomaterials. In contrast with classic elasto-plasticity, it accounts for soil non-linearity within the state boundary surface, for the elastic range of the soil is known to be very limited.

The hypoplastic model proposed by Mašín (2014)[17], in particular, is implemented within the framework of critical state soil mechanics and requires five basic material parameters φ_c, N, λ^*, κ^* and υ to be defined. The parameters have the same physical interpretation as for the Modified Cam clay model, and are thus easy to calibrate using standard laboratory experiments. As illustrated in Figure 2, the model parameters N and λ^* define the position and the slope of the isotropic normal compression line in the $\ln(1+e)$ vs $\ln(p/p_r)$ plane. The isotropic normal compression line is described using the equation

$$\ln(1+e) = N - \lambda^* \ln\left(\frac{p}{p_r}\right) \tag{1}$$

Where e is the void ratio and p_r = 1 kPa is a reference stress. Parameter κ^* controls the slope of the isotropic unloading line in the same plane and also of the isotropic compression line of overconsolidated soil. φ_c is the critical state friction angle, with identical meaning to that of any other critical state soil mechanics-based model. Finally, parameter υ controls the shear modulus.

Experimental data presented in Ragni et al. (2015)[13] using cyclic T-bar penetration in centrifuge tests (Stewart & Randolph 1994[18]) indicated that kaolin clay samples show a remoulding degree, $s_{u,rem}/s_{u,ini}$, where $s_{u,ini}$ is the initial, intact shear strength of the sample and $s_{u,rem}$ the remoulded value.

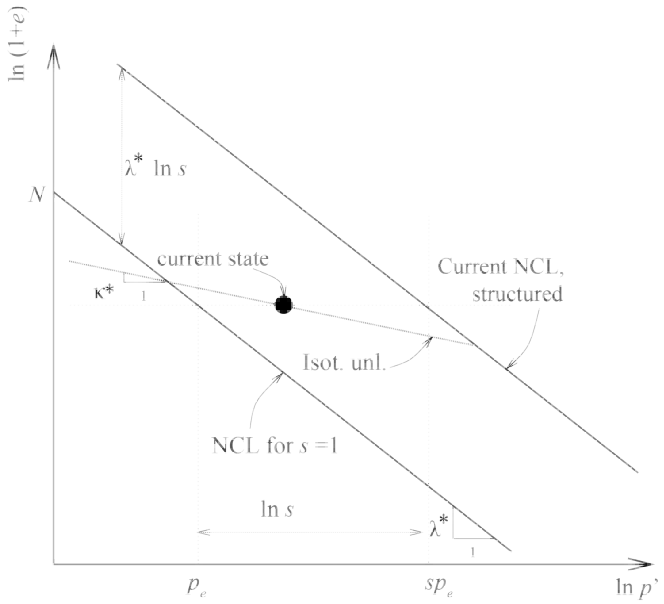

Figure 2: Hypoplastic bilogarithmic compression law for structured clay.

For this reason, the hypoplastic model by Mašín (2014)[17] was enhanced by the effects of the structure using a procedure developed in Mašín (2007)[16]. This enhancement requires three additional parameters, k, A and s_f, and the sensitivity s as a state variable. The normal compression line shown in Figure 2 then reads:

$$\ln(1+e) = N - \lambda^* \ln\left(\frac{p}{p_r}\right) + \lambda^* \ln(s) \tag{2}$$

Parameters A and k govern the sensitivity degradation rate, while s_f is the final value of the sensitivity. The set of parameters adopted for kaolin clay in the numerical simulations is given in Table 1. The coding of the version implemented in this work was made available on-line by Gudehus et al. (2008)[19], with free download of the code available from www.soilmodels.info.

The reader is referred to Ragni et al. (2015)[13] for a comprehensive description of the model equations and the complete calibration of the model for kaolin clay, where same soil and constitutive model were used to describe the problem of spudcan installation. Note that the model parameters imply undrained shear strength $s_u = 1.66w$ kPa/m, which is somewhat lower than the shear strength of the soil used in the centrifuge tests described later.

φ_c	N	λ^*	κ^*	υ	k	A	s_f
23°	1.195	0.0811	0.019	0.2	0.2	0.2	1

Table 1: Parameters of the hypoplastic model used in the simulations.

FROM TWO TO THREE DIMENSIONS: MAPPING PROCEDURE

A mapping of the deformed geometry, field variables and excess pore pressure was required to ensure continuity from the simulation of the penetration-consolidation to the multi-directional loading stage. Due to the mono-directional nature of the penetration, only a two-dimensional axisymmetric model was adopted. However, a three-dimensional model was required when simulating the following *VHM* investigation. The soil domain was thus created by revolving the axisymmetric model around a 180° angle, and chosen as 3D vertically and 6D horizontally (D is the spudcan diameter at its widest section, see Figure 3), in order to minimise boundary

effects and computational cost. In contrast, the soil domain was as large as 20*D* in the axisymmetric LDFE analyses of penetration and consolidation. Such a large domain was proven unnecessary for the *VHM* investigation, since three-dimensional analyses involving a larger soil domain offered a solution extremely close to the smaller domain (an average of -1.6% in the loading response), while at the same time dramatically increasing the computational cost by ~400%. The jack-up leg connected to the spudcan was intentionally not modelled in the three-dimensional analyses (Figure 3), in an effort to isolate the bearing capacity offered by the footing alone. A similar goal was also pursued in the following experimental investigation.

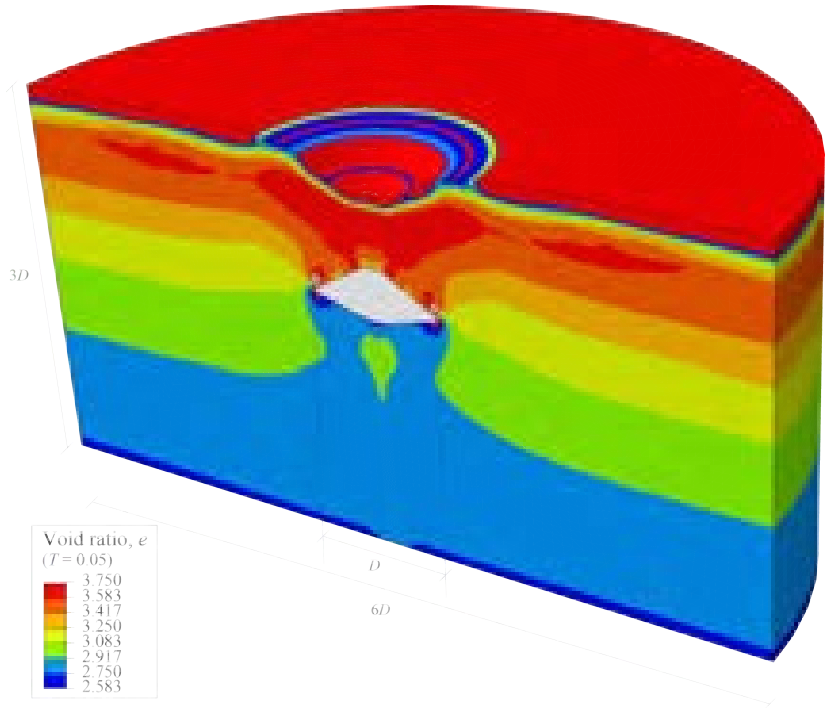

Figure 3: Illustration of the soil domain used in three-dimensional FE analyses and void ratio distribution after a period of consolidation $T = 0.05$.

Particular attention was dedicated to the mapping strategy, crucial to the continuity of field variables and excess pore pressure distribution. Once the spudcan was penetrated to the target depth with LDFE analyses, the resulting effective stresses and material properties were mapped to the integration points of the three-dimensional model, whereas the excess pore pressures were mapped to the nodes. The mapping strategy was such that every integration point and node of the three-dimensional model was searched in the axisymmetric model, by conversion of its three-dimensional coordinates to the axisymmetric corresponding counterpart. Then, each field variable was interpolated within the eight-node axisymmetric element which contains the integration point or the node. A mesh density similar to that of the axisymmetric model is desirable to minimise the error in interpolation. For the limited volume of soil replacing the leg which was present in LDFE analyses, it was assumed that the field variables were equal to those at the nearest integration point or node.

VHM INVESTIGATION WITH SSFE ANALYSES

The determination of the combined *VHM* bearing capacity required Small Strain Finite Element (SSFE) analyses only, given the small soil strains and consequent very limited mesh distortion, compared to the large deformation occurring during penetration.

Roughly 15,000 elements were used to discretise the soil domain shown in Figure 3. The minimum element size around the spudcan was 0.045*D*; further simulations reducing this value to 0.02*D* proved to have a marginal effect of 1% while, at the same time, increasing the computational effort by 700%. Further reduction of the element size in relation to the spudcan displacements is thought to generate excessive mesh distortion (Yi et al. 2014[20]) and cause analysis instability. For numerical stability and computational efficiency, the spudcan-soil interaction was simplified with a tie constraint, which tends to overestimate the capacity. However, further analyses involving frictionless contact showed a marginal effect (2.5% difference in pure rotation) on the magnitude of the combined bearing capacity.

DEFINITION OF THE YIELD SURFACE

Swipe tests were carried out in order to investigate the combined bearing capacity of the spudcan, following spudcan penetration to the target depth $w/D = 1$ and consolidation under constant vertical load. In the swipe tests, firstly proposed by Tan (1990) [21], a horizontal displacement u, a rotation θ, or a combination of both was applied, while the spudcan depth w was held constant, so as to generate load paths where V gradually reduced as the response in H and M increased. Provided a sufficiently high ratio of elastic over plastic stiffness of the soil (Tan 1990[21], Martin 1994[22], Martin & Houlsby 2000[9]), such load paths are thought to closely track the yield surface. All the swipe tests started from either V_0 *or* V_0^* (with $H = M = 0$) and moved along different paths of the three-dimensional surface, according to the $u{:}D\theta$ ratio, so to determine the capacity surface in the *VH* and *VM* planes. When the *HM* response of each swipe was plotted at constant V values (i.e. sectioning the yield surface parallel to the *H-M* plane at regular intervals along the V axis), the surface eccentricity was observed, which ultimately offered a comprehensive picture of the yield surface in the *VHM* space.

In order to interpret the results, the following equation to describe the shape of the yield surface in the *VHM* space was used, which generalises the version originally proposed by Martin & Houlsby (2000)[9], to account for the tensile side and the curvature of the surface:

$$f = \left(\frac{H}{h_0 V_0}\right)^2 + \left(\frac{M/D}{m_0 V_0}\right)^2 - \frac{2e_s HM/D}{h_0 m_0 V_0^2} + \\ -\left(\frac{(\beta_1+\beta_2)^{(\beta_1+\beta_2)}}{(\beta_1^{\beta_1}\beta_2^{\beta_2})}\frac{1}{(1+\chi)^{\beta_1}(1+\chi)^{\beta_2}}\right)^2\left(\frac{V}{V_0}+\chi\right)^{2\beta_1}\left(1-\frac{V}{V_0}\right)^{2\beta_2} = 0 \quad (3)$$

where h_0 is the peak of horizontal over vertical capacity in the *VH* ($M = 0$) plane, m_0 is the peak of moment over vertical capacity in the *VM* ($H = 0$) plane, e_s represents the eccentricity of the surface in *HM* plane and χ is the ratio of peak tensile over compressive capacity. β_1 and β_2 are responsible for the curvature of the surface. If a non-vertical force term Q is defined as:

$$Q^2 = \left(\frac{H}{h_0}\right)^2 + \left(\frac{M/D}{m_0}\right)^2 - \frac{2e_s HM/D}{h_0 m_0} \quad (4)$$

then Equation 3 can be simplified and re-written as:

$$f = \left(\frac{Q}{V_0}\right)^2 - \left(\frac{(\beta_1+\beta_2)^{(\beta_1+\beta_2)}}{(\beta_1^{\beta_1}\beta_2^{\beta_2})}\frac{1}{(1+\chi)^{\beta_1}(1+\chi)^{\beta_2}}\right)^2\left(\frac{V}{V_0}+\chi\right)^{2\beta_1}\left(1-\frac{V}{V_0}\right)^{2\beta_2} = 0 \quad (5)$$

and the results presented in the non-dimensional Q/V_0 - V/V_0 plane. The advantage of such simplification is that, provided the optimal set of parameters, all the tests should lay on the same curve.

EXPERIMENTAL SET-UP

Experimental swipe tests were carried out in the geotechnical drum centrifuge at the University of Western Australia at an acceleration of 200 g. The main advantage of the enhanced gravity level is the reproduction at a model scale of the same prototype stress field conditions.

The black rotating channel shown on the LHS of Figure 4 contains the soil sample, whereas the tool table positioned at the centre holds the *VHM* actuator with the testing equipment. Since the tool table can be manoeuvred independently of the rotating channel, equipment maintenance without interruption of the rotation of the channel is allowed (Stewart et al. 1998[23] for more details).

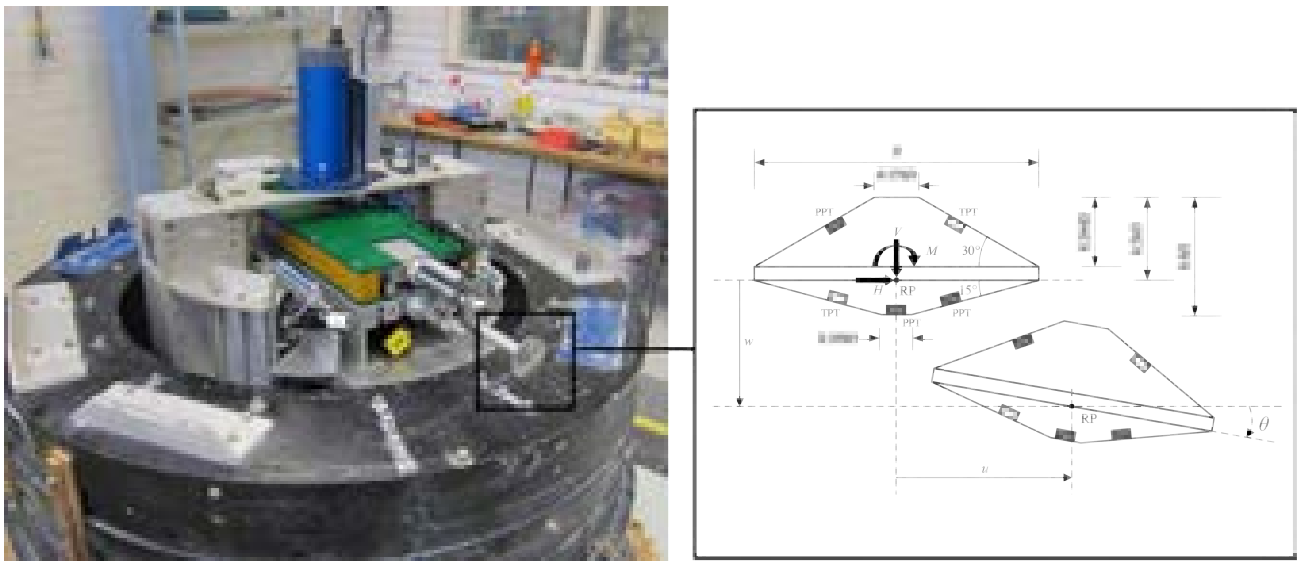

Figure 4: UWA drum centrifuge and *VHM* apparatus (LHS); spudcan geometry and load-displacement convention (RHS).

The geometry of the spudcan model used in the tests is shown on the RHS of Figure 4. The widest section of 60 mm represents a diameter D = 12 m in the prototype scale, due to the enhanced gravity level. The model featured two pore pressure transducers (PPT) and one total pressure transducer (TPT) at the bottom, and one of each at the top face, in order to monitor the evolution of excess pore pressure. The leg connecting the spudcan to the actuator was equipped with axial and bending gauges, which allowed axial, horizontal and bending loading to be calculated. Also, an aluminium shield protected the leg strain gauges; a soft silicon connection between the shield and the spudcan minimised the load transfer, allowing only the loading acting on the spudcan to be measured (Zhang et al. 2013[12]).

Commercially available kaolin clay was used for testing. The centrifuge channel was filled at 20 g with slurry prepared with a water content twice the liquid limit and consolidated in flight for about 11 weeks at 200 g, equivalent to ~ 8,500 years in prototype scale. A final sample height of 170 mm was achieved. Due to some mechanical issues with the centrifuge, the sample experienced stages where the water table was not above the soil surface. Nonetheless, the surface was constantly kept moist, and T-bar penetrations (section 5x20 mm, Stewart & Randolph 1994[18]) to characterise the sample confirmed a fairly uniform profile. The average undrained shear strength profile was estimated as $s_u = 2.18w$ kPa/m (w depth in m, prototype scale, Figure 5).

Note that lower $s_u = 1.66w$ kPa/m was adopted in the numerical model, which was performed on the assumption of the targeted normally consolidated soft clay profile.

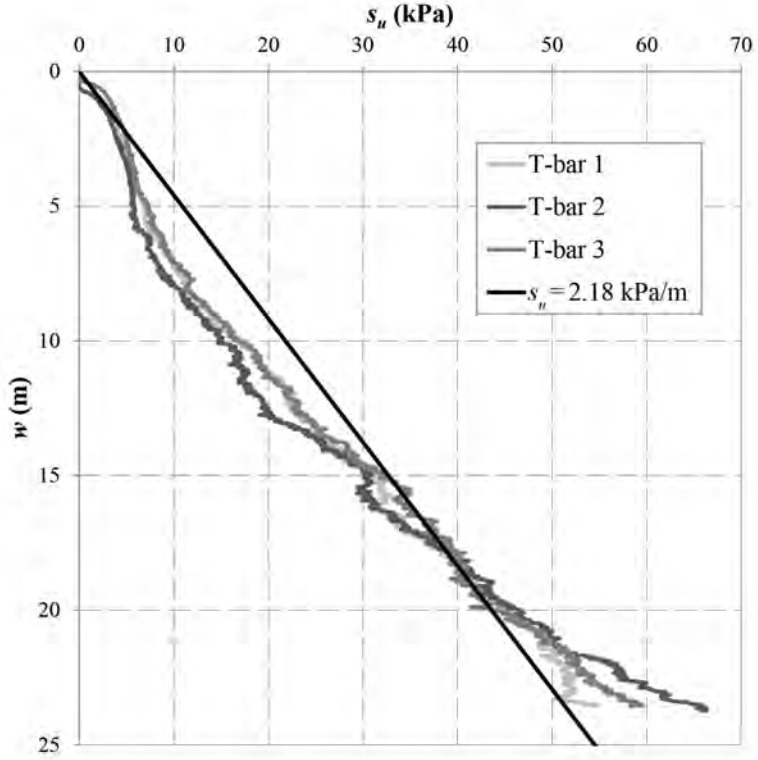

Figure 5: T-bar profiles in kaolin clay.

RESULTS AND DISCUSSION

VERTICAL PENETRATION

The first requirement for the numerical simulations was to simulate the initial stage of vertical penetration and following consolidation. All the analyses were started from an initial embedment $w/D = 0.5$ for stability purposes; further investigation with reduced embedments led to identical results at deeper penetrations, while at the same time increasing numerical instability considerably (Ragni et al. 2016[24]).

The dashed lines of Figure 6a represent the penetration profiles in terms of V against normalised penetration w/D. The reference case 'Num Ref' shows a continuous penetration to $1.8D$ with no interruption, whereas in two other cases the penetration was stopped at $1D$ to allow for consolidation to take place, by holding the load V just achieved. Table 2 shows how the study focussed on two values of the dimensionless consolidation time $T = c_v t/D^2 = 0.01; 0.05$, where c_v is the coefficient of vertical consolidation and t is the dimensional time. The coefficient of consolidation c_v measured experimentally via oedometer test was empirically interpolated as:

$$c_v = \sqrt{\left(1 + 0.14\sigma_v^{'}\right)} \tag{6}$$

The units of c_v and σ_v' (vertical effective stress assuming specific weight $\gamma' = 7.5$ kN/m^3) are m^2/year and kPa, respectively. Due to the extremely low c_v (~3.68 m^2/year at $w/D = 1$), $T = 0.01; 0.05$ yield values of t which are only realistic from an operational condition point of view. However, the findings presented below become relevant even for the installation case, in the event of more permeable soils.

Vertical Penetration			
Num	**Exp**	**$T = c_v t/D^2$**	***t* (prototype)**
Num Ref	-	N/A	N/A
Num $T = 0.01$	Exp $T = 0.01$	0.01	~5 months
Num $T = 0.05$	Exp $T = 0.05$	0.05	~2 years

Table 2: Summary of vertical penetration tests.

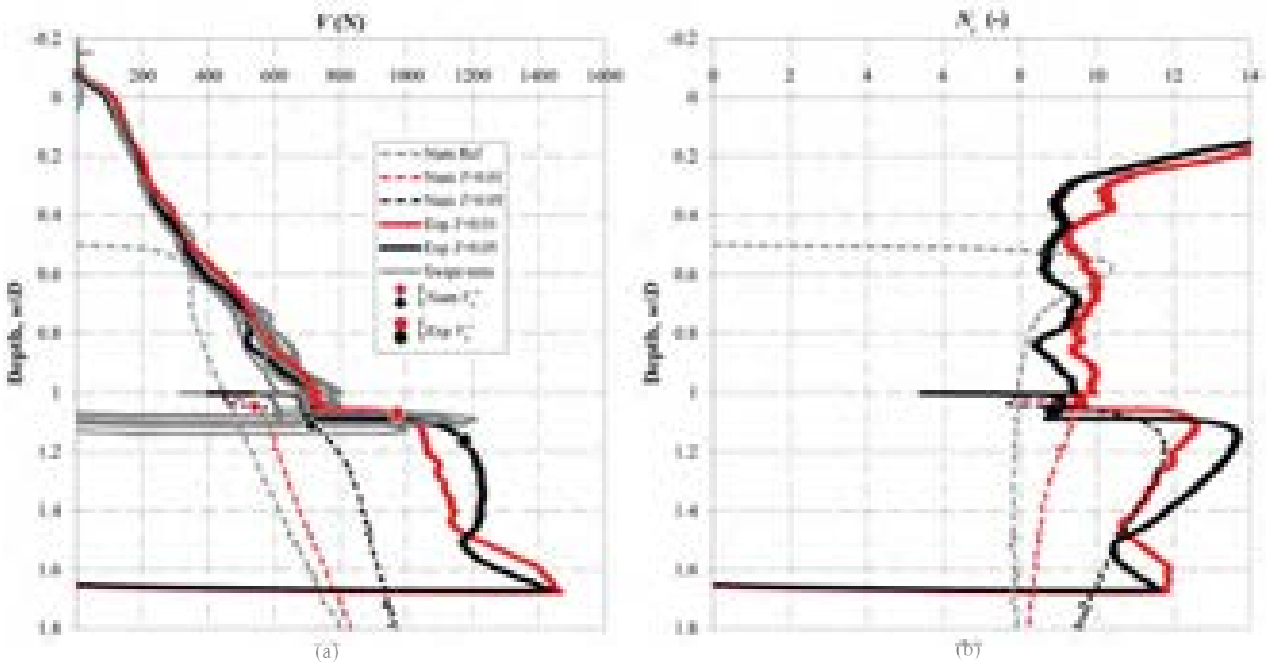

Figure 6: Spudcan penetration profiles and increase due to consolidation in terms of (a) vertical load *V*, and (b) bearing capacity factor N_c for numerical and experimental cases. Note that the soil in experiment had higher undrained shear strength s_u (2.18*w* kPa/m) than in the numerical model (1.66*w* kPa/m).

Further penetration post-consolidation identified increased bearing capacities $V_0^*(T = 0.01) = 541.04$ kN and $V_0^*(T = 0.05) = 711.75$ kN, with an increase of 15% and 45% when compared to the reference bearing capacity V_0 at the corresponding depth. Figure 7 explains the reason behind such improvement in vertical bearing capacity: the evolution of the normalised excess pore pressure $B_q = \Delta u/q$ (bearing pressure $q = V/A_s$, A_s is the spudcan area at its widest section) clearly shows a progressive dissipation with increasing consolidation time *T*. This reduces the void ratio in the proximity of the spudcan (see for instance Figure 3) and thus generates an increase in undrained shear strength s_u, which ultimately causes the observed peaks.

The same penetration-consolidation-penetration tests were reproduced experimentally in the centrifuge for $T = 0.01$; 0.05 (solid profiles in Figure 6). The initial penetration was carried out at a constant displacement rate of 0.2 mm/s, so to guarantee undrained conditions (Finnie and Randolph, 1994[25]). Then, consolidation was achieved by switching to load-control for the times considered, after which penetration was resumed at 0.2 mm/s.

Increased bearing capacities $V_0^*(T = 0.01) = 981.12$ kN and $V_0^*(T = 0.05) = 1126.29$ kN were obtained. Figure 7 also reports the experimental dissipation curves measured at the spudcan tip PPT (see RHS Figure 4) relative to

the consolidation stage of reference and swipe tests for $T = 0.01;0.05$. When compared to the numerical cases, equivalent values of B_q are achieved at the end of each consolidation stage.
Although the higher $s_{u,exp}$ (2.18w kPa/m against $s_{u,num}$ = 1.66w kPa/m) is generating a discrepancy between the absolute values of numerical and experimental V_0^* values, two things should be clarified. First of all, the numerical simulations align extremely well with previous experimental penetrations from Zhang et al. (2013)[12], where comparable tests with the same soil and spudcan shape/dimensions were carried out. Secondly, when the experimental results are normalised by $s_{u,exp}$, i.e. plotted in Figure 6b in terms of bearing capacity factor $N_c = V/A_s s_u$, the N_c values are once again in line with previous experimental evidence from Zhang et al. (2014)[26], which offered an average N_c = 10. In light of the above mentioned points, the results from vertical penetrations can be confidently assumed as the starting point for the following *VHM* investigation.

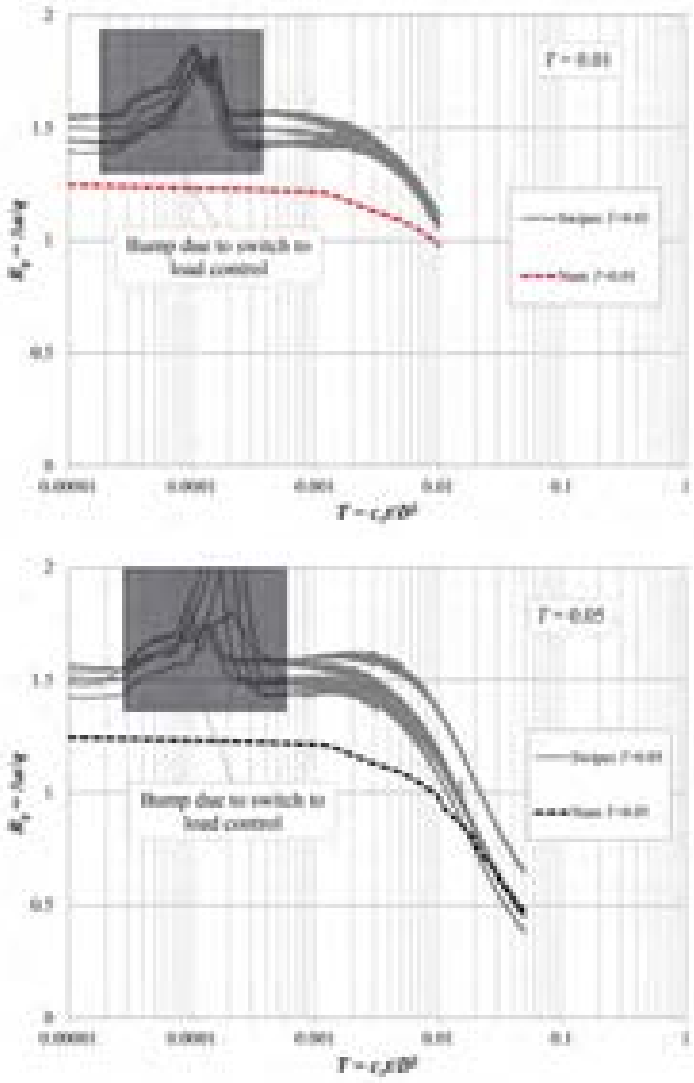

Figure 7: Excess pore pressure dissipation for (a) $T = 0.01$ and (b) $T = 0.05$.

MULTIDIRECTIONAL VHM CAPACITY
Swipe tests were used to determine the size and shape of the yield surface numerically. Keeping Equation 3 and 5 in mind, the previous section explained how a period of consolidation increased the vertical bearing capacity from V_0 to V_0^*. This was taken into account during the *VHM* investigation, by starting the swipe tests from V_0 = 448.06 kN, V_0^* ($T = 0.01$) = 541.04 kN and V_0^* ($T = 0.05$) = 711.75 kN for T = 0; 0.01; 0.05, respectively.

Different combinations of horizontal displacement u and rotation θ were applied to the spudcan in order to investigate different regions of the yield surface, as illustrated in Table 3.

T	$u/D\theta$	Swipe movement	
		u (mm)	θ (°)
0; 0.01; 0.05	∞	12	0
	0.95	9	9
	-0.095	-0.9	9
	-0.57	-5.4	9
	-1.15	-9	7.5

Table 3: Summary of numerical swipe tests.

Figure 8a,b,c present the swipe tests load paths in the normalised Q/V_0^*-V/V_0^* plane for increasing periods of consolidation. Through least square regression, the set of parameters of best fit that define the yield surface (Equation 3) was identified for each case. An increase in h_0 and m_0, more pronounced in the former than the latter, was observed. In particular h_0 increased by 21.7% and 33.9%, whereas m_0 only increased by 1.5% and 13.9%. Higher values for these two parameters indicate that not only is consolidation responsible for a higher vertical bearing capacity, but also increased horizontal and moment capacity. Moreover, the yield surface is modified in its shape, with a predominant effect on the H over M direction.

A comprehensive study on the spudcan tensile capacity, and how it is affected by consolidation, would have fallen beyond the scope of this work. For this reason, the value of $\chi = 0.6$ (best fit for $T = 0$) was maintained constant in all the cases for simplicity. $\chi = 0.6$ is also supported by experimental evidences from Zhang et al. (2014)[26]. The list of parameters for each T is summarised in Table 4.

Figure 8d,e,f show the results in the normalised H/V_0^*-M/DV_0^* plane. The black dashed lines represent sections of the yield surface at constant $V = 0.4$; 0.5; 0.6; 0.7; 0.8 V_0 (or V_0^*). The eccentricity e_s was determined from the plots: the value decreased from $e_s(T = 0) = 0.189$ to $e_s(T = 0.01) = 0.150$ and $e_s(T = 0.05) = 0.131$. This denotes a trend where the mutual influence between sliding (H) and rotational (M) failure mechanisms (see Ragni et al. 2017[27]) becomes weaker with rising V. Comparable reduction in e_s was presented in Zhang et al. (2014[26]), in which case, however, the increase in V was generated by deeper spudcan embedments.

Finally, a value of $\beta_2 = 0.8$, rather than $\beta_2 = 1$ as adopted for the experimental results, was assumed in order to optimise the fitting exercise of the numerical results (with one possible reason being the difference in interface conditions). $\beta_2 = 0.8$ generates a slight change in the curvature of the yield surface. However, this is a secondary aspect in the definition of the combined VHM capacity, and at the same time ensured an accurate estimation of far more important parameters h_0 and m_0, which govern the size of the surface.

T	h_0		m_0		e_s		χ		β_1		β_2	
	Num	Exp	Num	Exp	Num	Exp	Num	Exp	Num	Exp	Num	Exp
0	0.280	0.198*	0.137	0.092*	0.189	0.244*	0.6	0.6*	1	1*	0.8	1*
0.01	0.341	0.284	0.139	0.115	0.150	0.150	0.6	0.629	1	1	0.8	1
0.05	0.375	0.346	0.156	0.134	0.131	0.110	0.6	0.584	1	1	0.8	1

*After Zhang et al. (2014)[26].

Table 4: Parameters defining the yield surface for increasing $T = 0$; 0.01; 0.05.

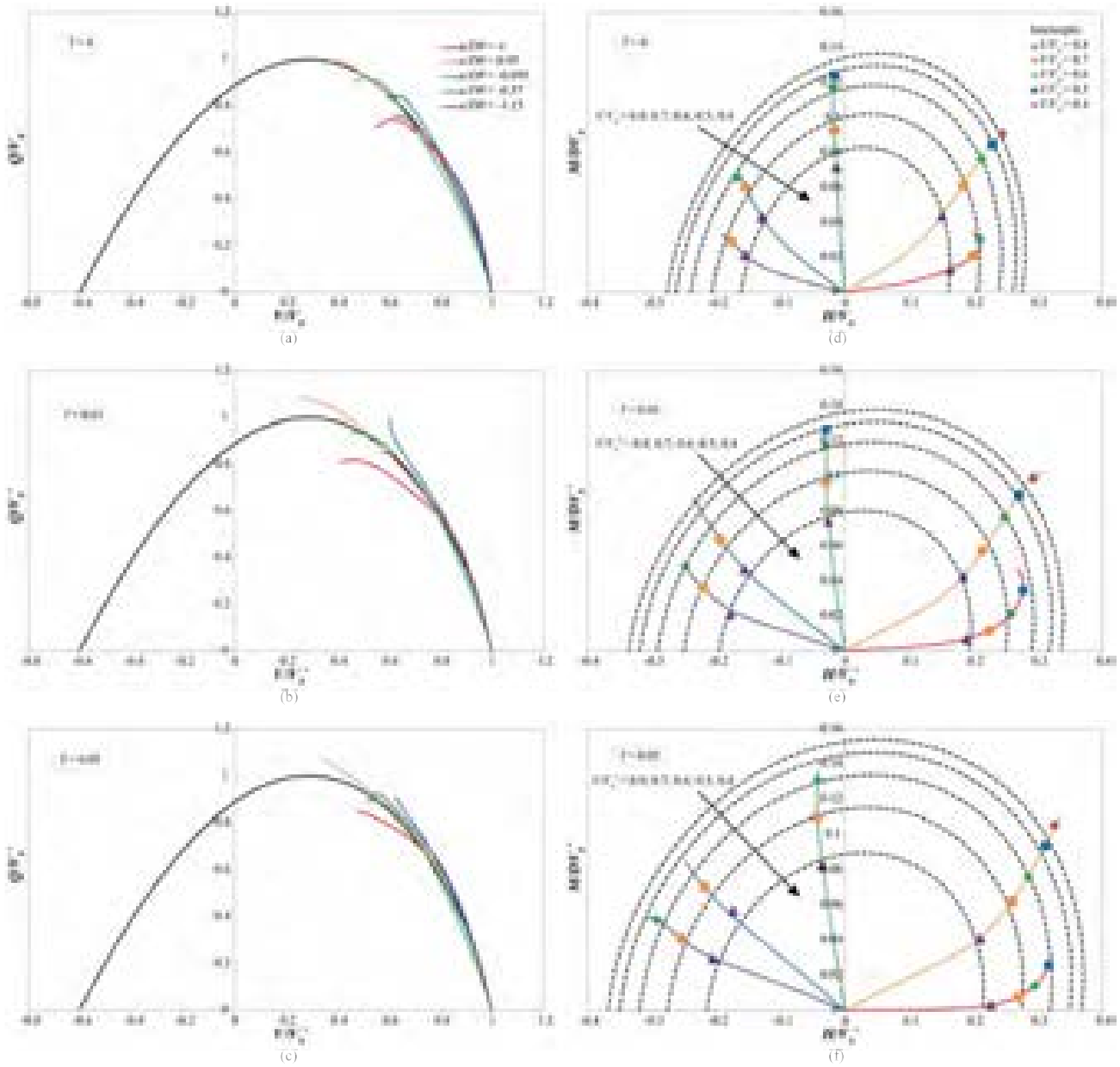

Figure 8: Numerical swipe test load paths and resulting yield surface in the (LHS) V/V_0^*-Q/V_0^* plane for (a) T=0; (b) T=0.01; (c) T=0.05, and (RHS) H/V_0^*-$M/D\ V_0^*$ plane for (d) T=0; (e) T=0.01; (f) T=0.05.

The numerical swipe tests for $T = 0.01$; 0.05 were then reproduced experimentally and are summarised in Table 5. As for the vertical penetration, the tests were carried out at a rate such that undrained conditions were guaranteed. The starting point was $V = V_0^*$ ($H = M = 0$), rather than V_0, to overcome an experimental shortcoming highlighted in Ragni et al. (2017)[27], where the load paths initially moved within the yield surface, losing relevant information regarding the yield surface. The swipe tests from Zhang et al. (2014)[26] were used as a benchmark for $T = 0$, since the same testing configuration was adopted.

The results shown in Figure 9a,b confirmed the trend already observed in the numerical simulation; for $T = 0.01$; 0.05, h_0 increased 43.4% and 74.7% when compared to the case with no consolidation (Zhang et al. 2013[12]); whereas increases of 25% and 45.7% were yielded for m_0.

$\chi(T = 0.01) = 0.629$ and $\chi(T = 0.05) = 0.584$ obtained from least square regression also aligned extremely well with both previous experimental experience from Zhang et al. (2013[12], 2014[26]) and numerical evidences presented above. Further investigation on the tensile segment of the surface would, however, be required to assess the exact role of consolidation on the spudcan tensile capacity.

T	$u/D\theta$	Swipe movement		Velocities		Swipe t (s)
		u (mm)	θ (°)	u' (mm/s)	θ' (°/s)	
0.01; 0.05	∞	12	0	0.4	0	30
	0.95	9	9	0.4	0.4	22.5
	-0.095	-0.9	9	-0.04	0.4	22.5
	-0.57	-5.4	9	-0.24	0.4	22.5
	-1.15	-9	7.5	-0.4	0.33	22.5

Table 5: Summary of experimental swipe tests

The experimental results in the H/V_0^*-M/DV_0^* plane for $T = 0.01$; 0.05 are presented in Figure 9c,d. As for the numerical counterpart, a more significant expansion of the yield surface in the H direction with increasing T is observed. The same trend is also noted in terms of eccentricity, with Zhang et al. (2013)[12] providing $e_s = 0.244$ for the case without consolidation, which is shown here to reduce to 0.150 and 0.11 for $T = 0.01$; 0.05, in excellent agreement with the numerical results. The full set of parameters for the experimental cases are also summarised in Table 4 and compared to the numerical counterpart.

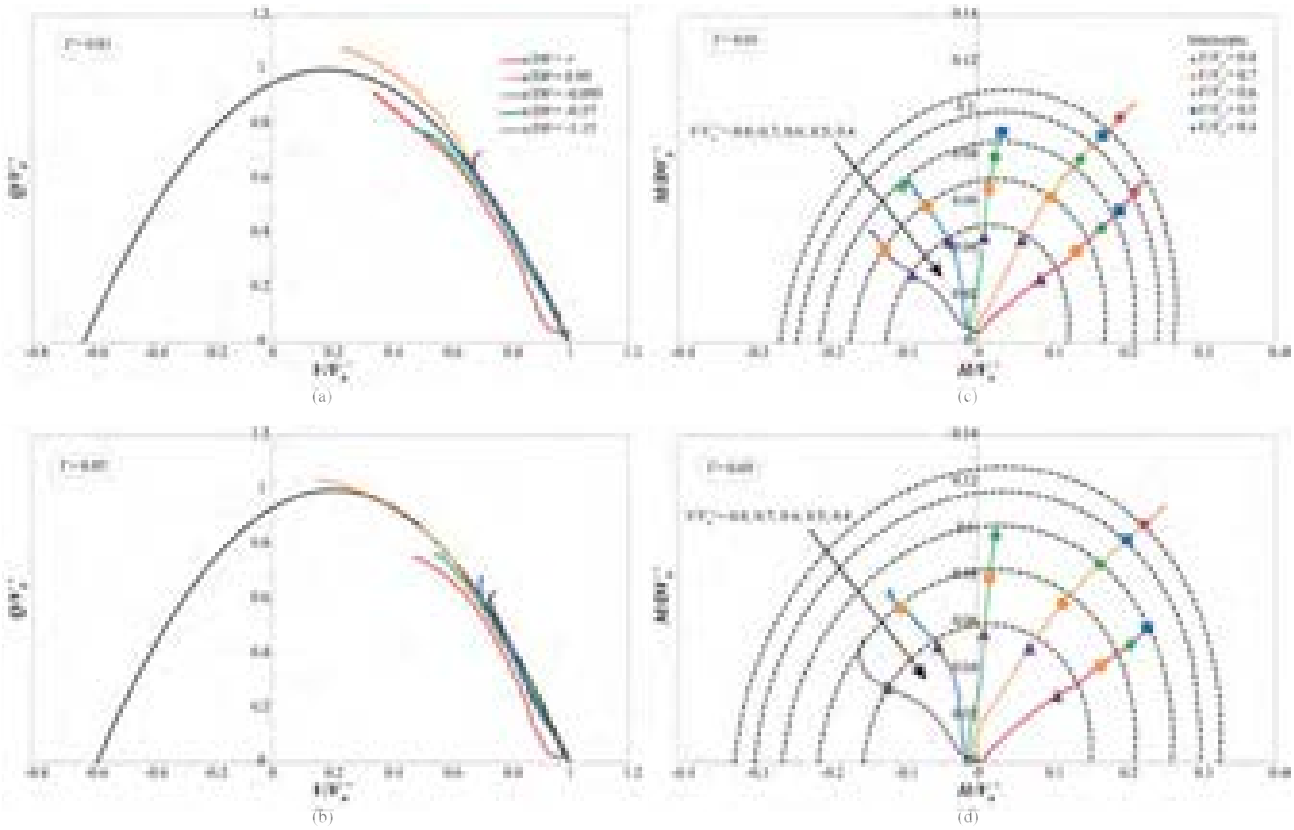

Figure 9: Experimental swipe test load paths and resulting yield surface in the (LHS) V/V_0^*-Q/V_0^* plane for (a) T=0.01; (b) T=0.05, and (RHS) H/V_0^*-$M/D\,V_0^*$ plane for (c) T=0.01; (d) T=0.05.

CONCLUSIONS

A combined numerical and centrifuge experimental study on the effects of consolidation on the spudcan undrained combined *VHM* capacity on fine-grained soil was presented. State-of-the-art numerical simulations allowed coherence of the analyses, with field variables and excess pore pressures continuously tracked from the early stage of vertical penetration to the final multi-directional loading stage.

A period of consolidation was demonstrated to influence the spudcan *VHM* capacity. In particular, increase in the parameters governing to the size of the yield surface highlighted the fact that not only does consolidation increase the surface, but also modifies its shape, i.e. the improvement is different in different loading directions. The increase in the *H* direction, in particular, was seen to be more pronounced than *M*, and comparable to the expansion in the *V* direction. The eccentricity of the surface in the *H-M* plane decreased considerably with increasing consolidation time, hinting to a reduction in the *HM* interaction for higher *V* values.

The experimental validation of the numerical results in a geotechnical centrifuge offered the same qualitative trend in terms of enhancement of the *VHM* capacity with consolidation, although the absolute values did not fully agree (which is caused in part by different undrained shear strength profiles of the soil in the experiments and the numerical model).

Further study would be required to properly assess the effects of consolidation on the spudcan tensile capacity. Once an optimal correlation is defined, a procedure to be used during site-specific assessment for the estimation of the increase in *VHM* capacity due to consolidation can be proposed. Considering the current lack of information, the ultimate goal is to propose a simple formulation to be included in the ISO (2015)[1] guidelines, where basic designing parameters would be sufficient to underpin the estimation of *VHM* capacity enhancement.

ACKNOWLEDGEMENTS

This work forms part of the activities of the Centre for Offshore Foundation Systems (COFS), which is supported by the Lloyd's Register Foundation as a Centre of Excellence and currently forms one of the primary nodes of the Australian Research Council (ARC) Centre of Excellence for Geotechnical Science and Engineering. Lloyd's Register Foundation invests in science, engineering and technology for public benefit, worldwide. This research was supported by ARC DP110101603.

REFERENCES

[1] International Organization for Standardization (ISO) - Petroleum and natural gas industries - Site-specific assessment of mobile offshore units - Part 1: Jack-ups. Geneva, Switzerland, 2015.

[2] Butterfield R, Ticof J - Design parameters for granular soils (discussion contribution). In: Proceedings, 7th ECSMFE. UK, 1979:361-374.

[3] Schotman, GJM - The effects of displacements on the stability of jackup spudcan foundations. In: Proceedings, Offshore Technology Conference. Texas, 1989.

[4] Nova R, Montrasio L - Settlements of shallow foundations on sand, Géotechnique. 1991:41(2):243-256.

[5] Dean ETR, James RG, Schofield AN, Tsukamoto Y – Theoretical modelling of spudcan behaviour under combined load, Soils and Foundations. 1997: 37(2):1-15.

[6] Cassidy MJ, Houlsby GT - On the modelling of foundations for jack-up units on sand. In: Proceedings, Offshore Technology Conference. Texas, 1999.

[7] Bienen B, Byrne BW, Houlsby GT, Cassidy MJ - Investigating six-degree-of-freedom loading of shallow foundations on sand, Géotechnique. 2006:56(6):367-379.

[8] Salciarini D, Tamagnini C. - A hypoplastic macroelement model for shallow foundations under monotonic and cyclic loads, Acta Geotechnica. 2009:4(3):163-176.

[9] Martin CM, Houlsby GT - Combined loading of spudcan foundations on clay: laboratory tests, Géotechnique. 2000:50(4):325-338.

[10] Martin CM, Houlsby GT - Combined loading of spudcan foundations on clay: numerical modelling, Géotechnique. 2001:51(8):687-699.

[11] Zhang Y, Bienen B, Cassidy MJ, Gourvenec S - The undrained bearing capacity of a spudcan foundation under combined loading in soft clay, Marine Structures. 2011:24(4):459-477.

[12] Zhang Y, Bienen B, Cassidy MJ - Development of a combined VHM loading apparatus for a geotechnical drum centrifuge, International Journal of Physical Modelling in Geotechnics. 2013: 13(1):13-30.

[13] Ragni R, Wang D, Mašín D, Cassidy MJ, Bienen B - Modelling the effects of pauses during spudcan penetration on further installation behaviour. In: Proceedings, The Jack-up Platform Conference. UK, 2015.

[14] Hu Y, Randolph MF - A practical numerical approach for large deformation problems in soil, International Journal for Numerical and Analytical Methods in Geomechanics. 1998:22(5):327-350.

[15] Wang D, Bienen B, Nazem M, Tian Y, Zheng J, Pucker T, Randolph MF - Large deformation finite element analyses in geotechnical engineering, Computers and Geotechnics. 2015:65:104-114.

[16] Mašín D - A hypoplastic constitutive model for clays with meta-stable structure, Canadian Geotechnical Journal. 2007:44(3):363-375.

[17] Mašín D - Clay hypoplasticity model including stiffness anisotropy, Géotechnique. 2014:64(3):232-238.

[18] Stewart DP, Randolph MF - T-bar penetration testing in soft clay, Journal of Geotechnical Engineering. 1994:120(12):2230-2235.

[19] Gudehus G, Amorosi A, Gens A, Herle I, Kolymbas D, Mašín D, Muir Wood D, Nova R, Niemunis A, Pastor M, Tamagnini C, Viggiani G - The soilmodels.info project, International Journal for Numerical and Analytical Methods in Geomechanics. 2008:32(12):1571-1572.

[20] Yi JT, Zhao B, Li YP, Yang Y, Lee FH, Goh SH, Wu JF - Post-installation pore-pressure changes around spudcan and long-term spudcan behaviour in soft clay, Computers and Geotechnics. 2014: 56:133-147.

[21] Tan FSC - Centrifuge and theoretical modelling of conical footings on sand, Ph.D. thesis, Cambridge University, UK, 1990.

[22] Martin CM - Physical and numerical modelling of offshore foundations under combined loads, PhD Thesis. University of Oxford, UK, 1994.

[23] Stewart DP, Boyle RS, Randolph MF - Experience with a new drum centrifuge, In: Proceedings, International Conference Centrifuge. Japan, 1998:1:35-40.

[24] Ragni R, Wang D, Mašín D, Bienen B, Cassidy MJ, Stanier SA - Numerical modelling of the effects of consolidation on the jack-up spudcan penetration, Computers and Geotechnics. 2016:78:25-37.

[25] Finnie IMS, Randolph MF - Punch-through and liquefaction induced failure of shallow foundations on calcareous sediments. In: Proceedings, International Conference on Behaviour of Offshore Structures. USA, 1994:217-230.
[26] Zhang Y, Cassidy MJ, Bienen B - A plasticity model for spudcan foundations in soft clay, Canadian Geotechnical Journal. 2014:51(6):629-646.
[27] Ragni R, Bienen B, Wang D, Mašín D, Cassidy MJ - Numerical modelling of the effects of consolidation on the undrained spudcan capacity under combined loading in silty clay, Computers and Geotechnics. 2017:86:33-51.